Mechanics of Interaction and Atomic-Scale Wear of Amplitude Modulation Atomic Force Microscopy Probes

ARTICLE *in* ACS NANO · MARCH 2013

Impact Factor: 12.88 · DOI: 10.1021/nn305901n · Source: PubMed

4 AUTHORS, INCLUDING:

David S. Grierson
University of Wisconsin–Madison
29 PUBLICATIONS **737** CITATIONS
SEE PROFILE

Kevin T. Turner
University of Pennsylvania
97 PUBLICATIONS **1,246** CITATIONS
SEE PROFILE

Robert W Carpick
University of Pennsylvania
221 PUBLICATIONS **6,338** CITATIONS
SEE PROFILE

Mechanics of Interaction and Atomic-Scale Wear of Amplitude Modulation Atomic Force Microscopy Probes

Vahid Vahdat,[†] David S. Grierson,[‡,§] Kevin T. Turner,[†] and Robert W. Carpick[†,*]

[†]Department of Mechanical Engineering and Applied Mechanics, University of Pennsylvania, Philadelphia, Pennsylvania 19104, United States, and [‡]Department of Mechanical Engineering, University of Wisconsin—Madison, Madison, Wisconsin 53706, United States. [§]Present address: systeMECH, LLC, Madison, Wisconsin 53703.

ABSTRACT Wear is one of the main factors that hinders the performance of probes for atomic force microscopy (AFM), including for the widely used amplitude modulation (AM-AFM) mode. Unfortunately, a comprehensive scientific understanding of nanoscale wear is lacking. We have developed a protocol for conducting consistent and quantitative AM-AFM wear experiments. The protocol involves controlling the tip—sample interaction regime during AM-AFM scanning, determining the tip—sample contact geometry, calculating the peak repulsive force and normal stress over the course of the wear test, and quantifying the wear volume using high-resolution transmission electron microscopy imaging. The peak repulsive tip—sample interaction force is estimated from a closed-form equation accompanied by an effective tip radius measurement procedure, which combines transmission electron microscopy and blind tip reconstruction. The contact stress is estimated by applying Derjaguin—Müller—Toporov contact mechanics model and also numerically solving a general contact mechanics model recently developed for the adhesive contact of arbitrary axisymmetric punch shapes. We discuss the important role that the assumed tip shape geometry plays in calculating both the interaction forces and the contact stresses. Contact stresses are significantly affected by the tip geometry while the peak repulsive force is mainly determined by experimentally controlled parameters, specifically, the free oscillation amplitude and amplitude ratio. The applicability of this protocol is demonstrated experimentally by assessing the performance of diamond-like carbon-coated and silicon-nitride-coated silicon probes scanned over ultrananocrystalline diamond substrates in repulsive mode AM-AFM. There is no sign of fracture or plastic deformation in the case of diamond-like carbon; wear could be characterized as a gradual atom-by-atom process. In contrast, silicon nitride wears through removal of the cluster of atoms and plastic deformation.

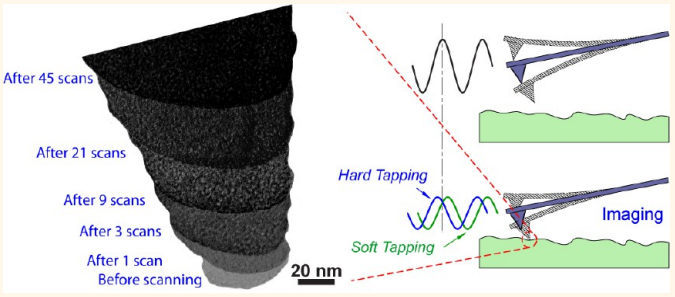

KEYWORDS: atomic-scale wear · AM-AFM · amplitude modulation · tapping mode · peak repulsive force · contact stress · contact mechanics

Since its revolutionary invention in 1986 by Binnig *et al.*,[1] the atomic force microscope (AFM) has become one of the most powerful tools in nanotechnology. It has been widely used for atomic-scale studies of chemical, biological, and engineering materials and has opened major opportunities for the advancement of nanoscale science. AFM has three primary operation modes for obtaining topographic images and material property measurements of samples: contact mode, noncontact mode, and intermittent contact or amplitude modulation AFM (AM-AFM, also known as tapping mode AFM). Over the past decade, AM-AFM has become the most popular imaging mode because of its minimal interaction with the sample, its relative ease of use, and its ability to obtain high-resolution images of materials. More recently, the use of oscillating probes has emerged in industry as a tool to facilitate nanoscale lithography, patterning, manipulation, surface characterization, and metrology.[2−7]

The mechanics of AM-AFM have been widely investigated by researchers since being introduced in 1987 by Martin *et al.*[8] Most of these studies have focused on understanding the dynamics of AM-AFM. Tip—sample interactions due to van der Waals forces, capillary forces, *etc.* have also been studied broadly, although there are aspects of tip—sample interactions still not yet fully understood. Continuum contact mechanics

* Address correspondence to carpick@seas.upenn.edu.

Received for review December 20, 2012 and accepted March 18, 2013.

Published online March 19, 2013
10.1021/nn305901n

models such as the Hertz,[9] Johnson–Kendall–Roberts (JKR),[10] and Derjaguin–Müller–Toporov (DMT)[11] are typically applied to estimate stresses and deformations at the tip–sample interface. These models assume, among other things, that the tip terminates in a paraboloidal shape. While such continuum mechanics models can be inaccurate when applied to nanoscale geometries, it can give reasonable values in several cases depending on the atomic structure of the tip and sample (according to Luan and Robbins[12]). Considering the lack of a general atomistic method and the unknown atomic structure of the tip and surface, continuum models are a significant improvement over existing state-of-the-art which often does not even address stresses in the contact during AM-AFM.

One of the major limitations for AFM is probe-tip blunting as a result of nanoscale wear. Wear during contact mode imaging has been examined in multiple studies, although it is yet to be fully understood.[13–18] AM-AFM was invented in part to reduce the problem of wear by nearly eliminating shear stresses acting on the tip due to sliding (intrinsically present in contact mode imaging) and reducing the total amount of time the tip interacts strongly with the sample. However, these advantages could be offset by the high frequency of oscillations, which can be on the order of hundreds of thousands of tip–sample contacts per second. Having many cycles of interaction is not intrinsically a problem by itself; however, the effect of any gradual process such as atom-by-atom removal or dislocation movement can scale up as a result. Therefore, tip wear can still be a limiting and costly factor in AM-AFM. Consequently, users have to periodically change probes to maintain high and consistent imaging resolution. However, a changing tip makes quantitative analysis of tip–sample interactions and sample property measurements challenging since tip-to-tip variations in shape and surface composition can be substantial.

Despite the importance of wear in AM-AFM, there are limited systematic studies on the phenomenon of tip wear itself. This motivates the present study, which is focused on developing a method for a controlled wear study with accurate determination and control of the tip–sample interaction forces and the resulting stresses. Another motivation is application-driven. In tip-based nanomanufacturing and metrology, which can involve AM-AFM operation of the probe, wear must be avoided for the process to be commercially viable. In contact mode, tip wear occurs during sliding and is influenced by the magnitude of stresses in the contact and the nature of the interfacial interactions. The causes of wear in AM-AFM can be quite different. While interfacial shear stresses are significantly reduced, the effects of cyclic loading and impact, uniquely related to repeated contact formation and breakage of AM-AFM, and the potential for excursions to high compressive forces may lead to distinct types of wear processes compared with contact mode AFM. Besides tip wear, tip contamination is also an important issue when it comes to reliable application of AFM,[19–24] but that requires a different comprehensive approach than what is discussed in this paper.

Existing studies of the wear of AM-AFM probes to date involved experimental investigations of wear reduction by using different tip materials[25,26] or by controlling the AM-AFM parameters[27] and modeling wear as a thermally activated process.[28] Su *et al.*[27] showed that operating with a relatively low amplitude ratio (tapping amplitude divided by free oscillation amplitude) has the advantage of reducing tip wear and permitting increased scanning speeds. That work sheds light on some of the experimental parameters affecting tip wear. However, it does not explain the wear process in a quantitative and predictive way since the tip geometry, the tip–sample deformation, and the attractive/repulsive force regimes are not included in the analysis.

Bassani and D'Acunto[28] performed analytical modeling of wear in AM-AFM. They considered wear as an irreversible atom-by-atom mass transfer from the sample to the tip as a result of adhesive interactions. The tip–sample interaction was modeled as a double-well potential, and mass transfer was treated as a transition between the two potential wells. They calculated wear volume as an exponential function of the energy barrier and predicted that the wear rate of a single atomic volume in the model depends on an Arrhenius rate law, which describes a thermally activated wear process. This model represents an important first step since previously such effects on the process of material removal had not been modeled from an atomistic point of view. However, the model neither considers atoms that can move from the tip to the sample nor does it consider diffusion of atoms from one region of the tip (or the sample) to another region without transferring across the interface. In addition, the model does not take into account the elastic deformation of the tip and sample and that mass transfer can occur *via* removal of clusters of atoms instead of single atoms. Although these complex issues are not addressed, this model is useful because it introduces a framework for modeling gradual wear processes in AM-AFM. To develop further insights, we must consider other parameters like contact stresses and radius that promote and determine the reaction rate besides the adhesion.

To highlight the key issues one might encounter and should take into account while studying wear in AM-AFM, in the following sections, we first discuss available analytical models to estimate contact forces and stresses and propose methods to apply them accurately by discussing parameters that may affect the results. We then explore the manifestation of these calculations in practice and examine the influence of the various

parameters involved by performing wear experiments with different probes as a function of different experimental parameters as summarized in Table 1.

RESULTS AND DISCUSSION

In AM-AFM, as the tip approaches and then retracts from a surface during a tapping cycle, it experiences two different force regimes: when far from the sample's surface, the tip experiences long-range attractive forces, mainly as a result of the van der Waals interaction with the sample; when close to the sample's surface, the tip experiences short-range repulsive forces as a result of Pauli and electrostatic repulsion and strong short-range attractive forces as a result of metallic, covalent, ionic, or hydrogen bonding interactions, for example. Capillary interactions can also contribute to attractive forces over intermediate separation ranges. The maximum repulsive (*i.e.*, normal) force is experienced by the tip during contact when it reaches its farthest distance away from its equilibrium position. At this point, the tip experiences the highest level of normal stress and overall strain energy, and it is thus at this position where the potential to inflict the damage to the tip is greatest. Therefore, the most relevant interaction force for studying AM-AFM wear is the peak repulsive force. Although in an "attractive only" mode, wear could potentially occur by atoms being pulled off from the tip, in fact, these long-range forces are small compared to forces needed to break bonds; so, this process is not considered to be significant.

Peak Repulsive Force. Although measuring the normal force acting on a tip in contact mode is straightforward, it is rather complicated in AM-AFM due to the dynamic and nonlinear tip−sample interactions. There have been several studies of force determination in AM-AFM. However, to date, a straightforward technique which is accurate over the entire range of tip−sample separations and can be used directly during the course of AM-AFM experimentation has not been established.

Katan *et al.*[29] extended a force inversion technique primarily derived for frequency modulation atomic force microscopy by Sader *et al.*[30] to AM-AFM. This technique was based on a point-mass and spring model of the AFM tip-cantilever and requires obtaining data for the amplitude and phase as a function of the tip−sample separation distance. Although this technique does not require any information to be provided regarding the tip geometry and solely depends on the experimental measurements of phase and amplitude as a function of *z*-motion, it is quite sensitive to small offsets of the phase data and miscalculates the interaction force in cases where the tip−sample interaction stiffness exceeds the cantilever stiffness.[31] In addition, it cannot be used in a straightforward, real-time manner by an AFM user during an experiment. Specifically, the interaction force cannot be deduced from the phase and amplitude images alone, as such images are acquired at a nominally fixed tip−sample distance. Rather, data corresponding to a range of tip−sample distances are required for the application of this method. These challenges make this technique unsatisfactory for the purpose of monitoring forces during wear studies.

Hu *et al.*[32] proposed closed-form equations for peak attractive and repulsive interaction forces derived from applying a nonlinear dynamical one-term harmonic balance method to the point-mass model. These equations are accurate over a wide range of experimental parameters in vacuum and air. Having closed-form equations to calculate peak interaction forces would be convenient for AFM users. However, these equations are limited to cases where the tip remains paraboloidal and requires that the tip radius be accurately measured experimentally.

In the present work, the equations developed by Hu *et al.* are used to approximate the peak repulsive force experienced by our AFM tips. Measurements of the tip radius are performed periodically using high-resolution transmission electron microscopy (HR-TEM) imaging and blind tip reconstruction (BTR), a method which is described later. The equation for the peak repulsive force, developed for the case of the DMT contact model (a justification for using the DMT contact model is discussed later), is as follows:

$$F_{\text{peak}}^{\text{rep}} \approx 2^{1/8}3^{-1/4}\pi^{3/4}(E^*\sqrt{R})^{1/4}(k/Q)^{3/4}A_0^{9/8}A_{\text{ratio}}^{9/8} \times\left\{(-1+\Omega^2)Q+\sqrt{\frac{1}{A_{\text{ratio}}^2}[\Omega^2+(1-\Omega^2)^2Q^2]-\Omega^2}\right\}^{3/4} - F_{\text{adhesion}}/2 \quad (1)$$

where E^* is the reduced Young's modulus, R is the tip radius, k is the cantilever spring constant, Q is the cantilever's quality factor for the primary flexural mode, A_0 is the free amplitude, A_{ratio} is tapping amplitude A divided by A_0, Ω is drive frequency ω divided by resonance frequency of the primary flexural mode ω_0, and F_{adhesion} is the adhesion force.[32] Here, F_{adhesion} is calculated using the DMT model:

$$F_{\text{adhesion}} = -2\pi wR \quad (2)$$

where w is the work of adhesion, which is determined independently by performing pull-off force measurements using tips of the same type from the same vendor, that is, composed of the same material as the tips studied in the wear experiment. This is described further below.

To verify the accuracy of the equation, one can use an online tool developed by Melcher *et al.*[33] and provided by http://nanohub.org, called the Virtual Environment for Dynamic AFM (VEDA). This tool numerically solves the Euler−Bernoulli partial differential equation of a thin cantilever beam to construct amplitude and phase approach curves and to calculate the peak repulsive/attractive forces for a given set of experimental parameters. It also provides a more

TABLE 1. Cantilever Properties and Experimental Parameters Used for Wear Experiments

cantilever	spring constant (N/m)	resonance rrequency (kHz)	free oscillation amplitude, A_0 (nm)	amplitude ratio, A_{ratio}
PPP_NCHR (Nanosensors), 20 nm DLC coating	42.5	303.4	50	0.5
NSC15 (MikroMasch), 10 nm SiN_x coating, tip 1	44.2	315.5	35	0.4
NSC15 (MikroMasch), 10 nm SiN_x coating, tip 2	49.7	337.6	23	0.4

accurate estimation of forces as it does not involve mathematical approximations used to derive eq 1.

Contact Mechanics Model and Average Normal Stress. Before calculating interaction forces and stresses in any contact problem, an appropriate contact mechanics model needs to be chosen. It is normally assumed that the tip and sample are composed of homogeneous, isotropic, and linear elastic materials and that the tip shape is a paraboloid. It is also assumed that deformations are small compared to the contact radius, which in turn is small compared to the tip's radius of curvature. One then needs to calculate the Maugis parameter and the nondimensional load and use the adhesion map proposed by Johnson and Greenwood[34] to select the proper contact mechanics model. As shown in the Methods section, our tip and sample interactions are best described by the DMT contact model. Using this model, the average normal stress, when the tip is at its farthest distance away from its equilibrium position, is calculated to be

$$\sigma_{avg}^{norm} = \frac{1}{\pi}\left(\frac{4E^*}{3R}\right)^{2/3}(F_{peak}^{rep} - F_{adhesion})^{1/3} \qquad (3)$$

Comparing this equation with eq 1, one can recognize that the dependence on tip radius is stronger in the stress calculation as compared to the repulsive force calculation. In eq 1, R is raised to the power of 1/8, while in eq 3, R is raised to $-5/8$ ($=-2/3 + (1/8)(1/3)$), a factor of 5 larger. It should be mentioned that the values of the force and stress are dominated by the first terms in eq 1 and 3; therefore, the dependence of the second term, $F_{adhesion}/2$, on R does not significantly contribute to the calculation of the force and stress. This shows how errors in the determination of the tip geometry (or deviation of the tip shape from paraboloidal) can greatly influence the stress calculation. As will be demonstrated in the following HR-TEM images, AFM tips are not always simple spheres or paraboloids and can have nanoscale roughness. Additionally, they are often not axisymmetric. Thus, imposing contact mechanics models that assume a simple tip shape can introduce significant errors in the calculation of the stress.

To mitigate this issue, in the present work, the average normal stress and correspondingly the contact radius and deformation are also calculated numerically by solving a general contact mechanics model proposed by Zhou *et al.*[35] for the adhesive contact of arbitrarily shaped axisymmetric punches. All of the classic contact mechanics models, including Sneddon's and Boussinesq's solutions, are special cases of the proposed solution. Equations 34, 35a, and 35b of ref 35 are used for this purpose. In these equations, the term $p(t)$, the adhesive interaction force function, is set to zero because of the fact that there is not a straightforward way to accurately determine the adhesive function for the AFM tips. Instead, the adhesion force is added to the peak repulsive force as is done for the Hertz model to lead to the results for the DMT model. Although here we are applying this concept to the arbitrary tip profiles which are not necessarily paraboloidal, it is the most straightforward approach that we can come up with at this point.

TABLE 2. Material Properties Used in Calculations of the Contact Properties[a]

	Young's modulus (GPa)	Poisson's ratio
UNCD	790 ± 30[37]	0.057 ± 0.038[37]
DLC	150 ± 30[36]	0.3 ± 0.05[38]
SiN_x	230 ± 50[39−42]	0.23 ± 0.05[39−42]

[a] Silicon nitride material properties are the average of different values reported in literature.[39−42]

To examine the applicability of the proposed wear protocol (described in the Methods section), one silicon probe (PPP_NCHR, Nanosensors) coated with a 20 nm thick diamond-like carbon (DLC) film and two 10 nm thick silicon-nitride-coated silicon probes (NSC15, MikroMasch) were tested. The counter surface was an ultrananocrystalline diamond (UNCD)[13−15] film deposited on a Si substrate (Aqua 25, from Advanced Diamond Technologies, Inc.). The 20 nm DLC coating was deposited on the silicon probes using a plasma immersion ion implantation and deposition process by Dr. K. Sridharan (University of Wisconsin—Madison, Center for Plasma-Aided Manufacturing).[36] The hydrogen content of the DLC film is about 41 atom %, and approximately 50−70% of the carbon structure is in the sp^3 state; this is known as a hydrogenated amorphous carbon (a-C:H) film. These experiments are performed using the Asylum MFP-3D AFM at a fixed relative humidity of 15% in a mixture of N_2 gas and humid air. The AM-AFM parameters, which are listed in Table 1 along with the cantilever properties, are chosen to scan the sample in the repulsive regime. The material properties used for calculating the Maugis parameter, the peak repulsive force, and the average normal stress are summarized in Table 2.

The HR-TEM images of the DLC and silicon-nitride-coated probes before any AFM scanning and after completing 1, 3, 9, 21, and 45 scans ($1 \times 1\ \mu m^2$, 512×512 pixels, 2 Hz scan rate) are presented in Figure 1 and Figure 2. The contrast difference between the silicon

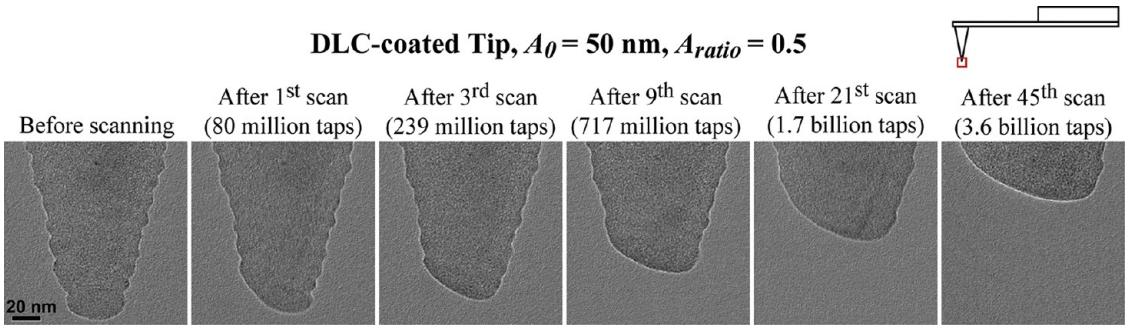

Figure 1. HR-TEM images of a DLC-coated silicon tip before any AFM imaging and after completing 1, 3, 9, 21, and 45 AM-AFM images on the UNCD sample.

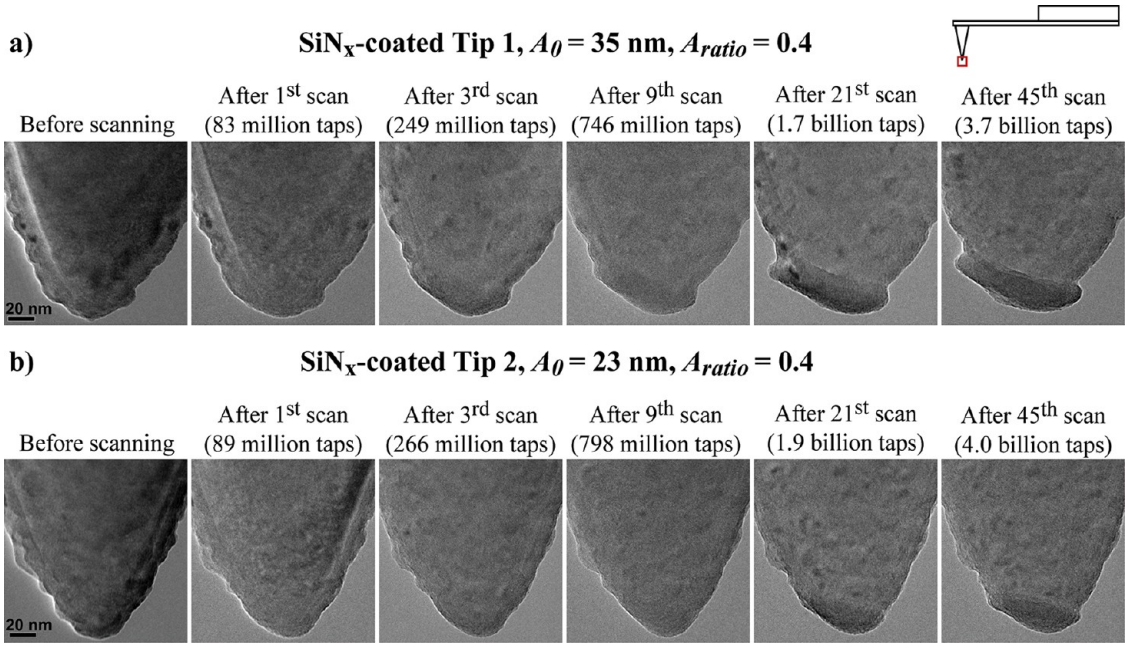

Figure 2. HR-TEM images of the two silicon-nitride-coated silicon tips before any AFM imaging and after completing 1, 3, 9, 21, and 45 AM-AFM images on the UNCD sample. (a,b) Two tips with different free oscillation amplitudes, A_0, and amplitude ratios, A_{ratio}.

and the respective amorphous coating is not present in these HR-TEM images. The specialty probe holder used for mounting the AFM probes in the HR-TEM allowed only limited sample tilt. Therefore, it was not always possible to tilt the crystalline silicon to an orientation of high symmetry (*i.e.*, high diffraction contrast).

The HR-TEM images show that wear in AM-AFM probes operating in repulsive mode can be significant even in the case of hard, wear-resistant materials like silicon nitride. Wear in silicon-nitride-coated tips occurs largely through plastic deformation, which is readily apparent from the bulging of the flattened tip and contrast changes at the apex in the rightmost images in Figure 2a,b. Darker contrast in TEM will occur when a material is compressed and becomes thicker in the direction of the TEM beam (the direction normal to the image). It can be seen that the end of the tip has also become wider where the contrast is darker. Thus, this indicates that a "pancaking" effect has occurred, consistent with plastically deformed material. Also, although silicon nitride is a brittle material, plasticity is well-known to occur in highly compressive stress states such as in nanoindentation of thin-film silicon nitride.[43−45]

Fragmentation of clusters of atoms could be another wear mechanism to explain the roughened tip apexes, which are observed in all of the worn silicon nitride tips' images (Figure 3). This increase in roughness is also quantified through measuring the roughness values of the tip apexes shown in Figure 3. To obtain an equivalent roughness of a flat surface, a parabola is fit to the tip profile captured from a TEM image, and then this best-fit parabola is subtracted from the actual tip profile over a 20 nm extent of the profile's length centered at the bottom of the tip (where it makes contact). The measured values show a decrease in the roughness of the DLC-coated tip and an increase in the roughness of the silicon-nitride-coated tips. This suggests that material removal in DLC is a gradual atom-by-atom process as reported previously in a contact mode AFM wear study,[17] while

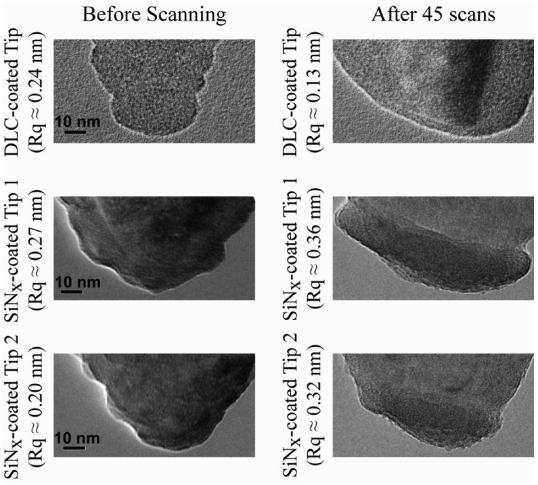

Figure 3. High-magnification HR-TEM images of the tip apexes before any scanning and after 45 scans. The roughness change of the silicon-nitride-coated tips can be observed in the images after 45 scans. The roughness values measured over 20 nm wide profiles of the tip apexes also show a decrease in the roughness of the DLC-coated tip and an increase in the roughness of the silicon-nitride-coated tips.

for silicon nitride tips, nanoscale clusters of silicon nitride are apparently removed. The exact reasons for the different behavior are unknown, but it may be a result of nanoscale subsurface crack formation and propagation to the surface. This is supported by the fact that silicon nitride has lower macroscopic fracture toughness, $K_{IC} \approx 6.3$ MPa·m$^{1/2}$,[46] than the DLC coating, $K_{IC} \approx 10.1$ MPa·m$^{1/2}$.[47] However, further investigation is required to fully understand this complex process.

In Figure 4, calculated peak repulsive forces as they evolve due to tip shape modification are plotted for all three tips. For each tip, there are three different plots corresponding to three different methods of calculating the peak repulsive force. The first is obtained by using eq 1 with $R = R_x$ (estimated by BTR from the topographic images using the fast scan direction, which is perpendicular to the cantilever axis here); the second using eq 1 with $R = R_y$ (estimated by comparing HR-TEM and BTR from the topographic images using the slow scan direction as described in the Methods section); and the third using VEDA, the online tool mentioned above, to verify our approach. R_y is used as the tip radius input for VEDA. In all cases, there is a close agreement between these two methods of force determination, and the VEDA results sit within the standard error of the forces calculated using eq 1. Also, if we more closely look at the case of the DLC-coated tip which has the highest variation in the peak repulsive force (from 90 nN at the beginning to 112 nN at the end using $R = R_y$), we can see that the tip radius changes from 22 to about 82 nm. In other words, the final tip radius is about 3.7 times larger than initial tip radius, while the final force is about 1.2 times larger than the initial force, supporting the fact that the peak repulsive force is not highly sensitive to the tip shape. Therefore, our approximation of fitting a

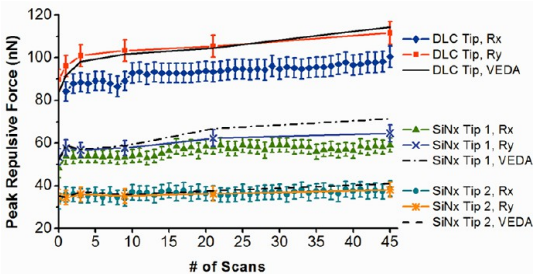

Figure 4. Peak repulsive forces calculated for all three tips based on the tip radii estimated by BTR from the height images' fast scan direction (R_x) and combined HR-TEM and BTR of the height images' slow scan direction (R_y). Peak repulsive forces are also calculated using VEDA for verification.

circle or a parabola to the tip shape to calculate force does not introduce significant error.

For all tips, a modest increase in the peak repulsive force is seen early in the wear test, followed either by a leveling off or a more gradual increase. The initial rapid increase is attributable to the rapidly increased tip size.

Average normal stresses *versus* the number of wear scans are plotted in Figure 5. There are three stress values for each tip obtained by using the DMT model: one calculated assuming a paraboloidal tip with $R = R_x$, one assuming $R = R_y$, and finally one where the model of Zhou *et al.* is applied to the axisymmetric tip shape based on the actual tip profile. The dramatic influence of ignoring the local details of the tip profile (by simply fitting a parabola/circle to the tip) is obvious for the SiN_x-coated tips and demonstrates that an accurate stress calculation requires consideration of the actual tip profile.

The calculated stresses using actual tip profiles of the SiN_x-coated tips are very large (beyond the elastic regime) because of the high local curvature at the contact as a result of considering the roughened tip. In other words, the asperity in contact is always rather sharp even though the entire tip gets generally blunter. Here, we assume elastic behavior for the stress calculation; since the stress values exceed the elastic regime and plastic behavior is observed particularly in the case of SiN_x-coated tips, the actual stresses are lower, and thus our calculated stresses are upper bounds. In contrast, the stresses calculated from parabola/circle fit provide a lower bound for the contact stresses as the tip and sample roughness are ignored.

Another difference between the wear behavior of DLC and silicon nitride can be observed in the change of their wear volume throughout the experiment. The volume loss due to wear for each of the tips *versus* number of taps is shown in Figure 6. The rate of wear reduces only slightly for DLC, while it decreases rapidly and reaches a plateau for silicon nitride. One thing to bear in mind when comparing different cantilevers is that the same number of wear scans does not mean the same number of tip−sample interactions since different cantilevers have different resonance and, consequently, drive frequencies. Therefore, in Figure 6,

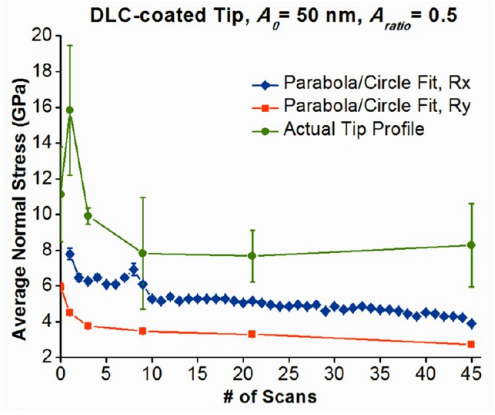

a)

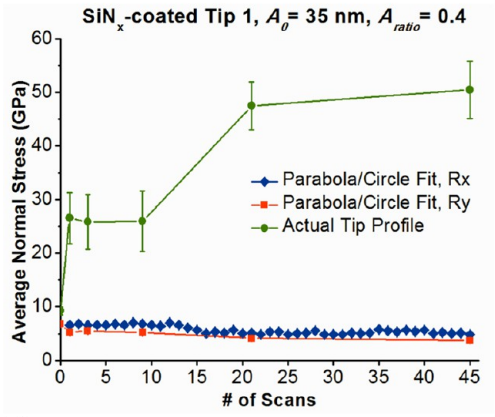

b)

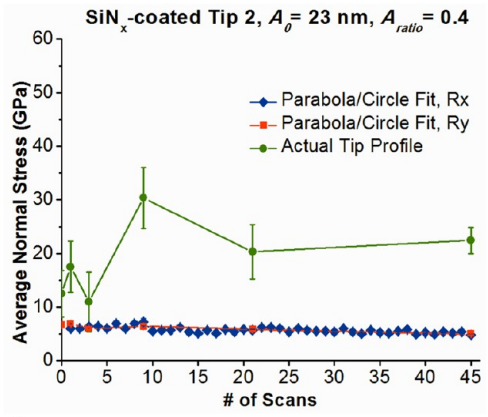

c)

Figure 5. Average elastic normal stress calculated for all three tips based on the tip radii estimated by BTR of the height images' fast scan direction (R_x), combined HR-TEM and BTR of the height images' slow scan direction (R_y) and the actual tip profile.

the wear volume for all three tips is plotted against the number of taps rather than the number of scans.

The different wear behavior for DLC and silicon nitride mentioned above can also be seen by plotting the average number of taps that is required to remove or plastically displace one atom of the tip (Figure 7). Note that the term "plastic displacement" is used here for silicon nitride tips because the volume displaced from the apex is not necessarily removed: some of it is plastically displaced to the side of the apex, leading to the bulging of the worn tip seen clearly in Figure 2a starting from the 21st scan. Here, it should be mentioned that the plot in Figure 6a for wear volume of DLC *versus* number of taps is nearly linear, whereas the plot in Figure 7a is clearly nonlinear. The nonlinearity in Figure 7a arises from the fact that, after 9 scans, subsurface silicon begins to wear, and thus there are a different number of atoms in a given cubic nanometer that are being removed. To estimate the number of atoms removed after 9 scans, worn volume of the subsurface silicon is calculated separately. The worn subsurface silicon is assumed to be cone-shaped, and the base diameter of this cone is estimated by inspecting HR-TEM images through the contrast difference between the DLC and silicon. There are two other complications that arise from the exposure of subsurface silicon at the contact interface. As after the ninth scan there is a combination of DLC and silicon interacting with the sample, the work of adhesion and reduced Young's modulus (E^*) will be different. To address this, we separately measured the work of adhesion between silicon and UNCD to be 30 $\pm$ 17 mJ/m^2, which is very similar to the work of adhesion between the DLC and UNCD, 31 $\pm$ 12 mJ/m^2. Therefore, we used the work of adhesion between silicon and UNCD, which has a larger uncertainty, for the ninth scan and after. Regarding the reduced Young's modulus, the combined modulus for DLC-UNCD is 137 $\pm$ 23 GPa and for Si-UNCD is 138 $\pm$ 19 GPa. These are indistinguishable within the uncertainty. For the ninth scan and after, we thus continued using the value of DLC-UNCD's reduced Young's modulus. Figure 7 shows that the average number of taps required to remove one atom of DLC (or one atom of DLC or silicon after 9 scans) ranges from 77 to 97, while the average number of taps required to remove or plastically displace one silicon nitride atom ranges from 240 to 30 000. In both cases, the number of taps required to remove atoms generally increases with the number of scans, except for a small decrease from 3 to 9 wear scans of the

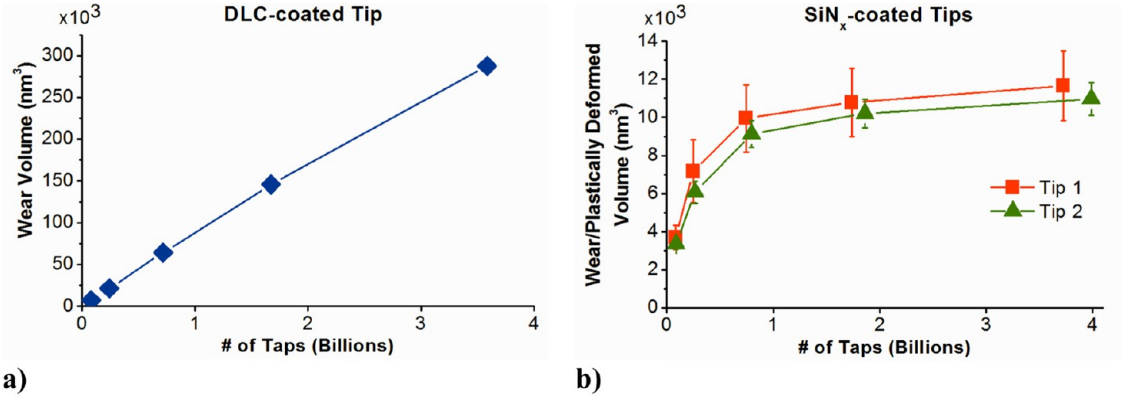

Figure 6. Wear volume as a function of number of taps for all three tips. For the DLC-coated tip shown in (a), the standard deviation of the measured wear volume is negligible in comparison to the wear volume itself and thus cannot be seen in the plot.

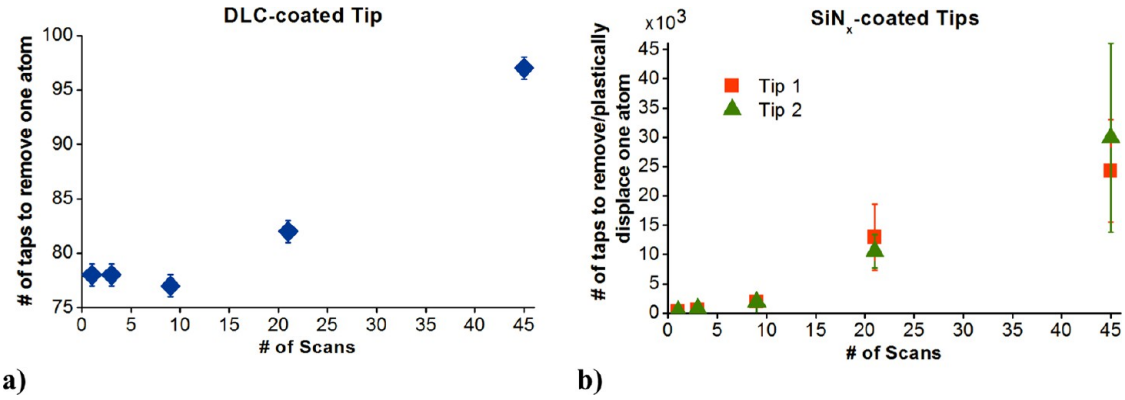

Figure 7. For all three tips, the number of taps to remove or plastically displace one atom as the tip wears out.

DLC-coated tips (Figure 7a), which suggests an accelerating wear process for DLC initially.

The increased wear rate of DLC compared with silicon nitride may have multiple origins. Once one or more bonds form between a tip atom and atoms on the surface of the sample, when the tip retracts, that tip atom may get left behind on the sample's surface (*i.e.*, strained bonds in the tip are preferentially broken). Therefore, higher wear could result if there are a greater number of atoms in the DLC tip compared to silicon nitride which are either weakly bonded or whose bond strength is easily lowered due to the presence of stress. Furthermore, the DLC may have a greater tendency to form covalent bonds (carbon–carbon bonds) with the UNCD surface as compared with silicon nitride (which would require Si–C or N–C bonds to form). This formation and breaking of such bonds is known to be affected not only by stress but also by environmental species. Finally, the observed plastic flow in the silicon nitride may result in a form of work hardening at the tip apex that makes it more difficult to remove or displace tip atoms. Further studies are needed to elucidate these mechanisms. Our results here provide clear qualitative observations of the characteristics of this nanoscale wear and also provide quantitative values for the forces, stresses, and wear volumes that need to be accounted for in a description of these mechanisms.

The significant wear observed in AM-AFM probes must, of course, be related to the average normal stress exceeding a threshold required for the failure of the tip materials, potentially in combination with interfacial chemical reactions that lead to removal of atoms. Thus, contact mechanics models used to calculate force and stress that assume fully elastic contact could be inaccurate. This suggests revisiting the solutions of force and stresses including the effects of plasticity, particularly in the case of AFM tips subjected to tapping conditions in the repulsive regime. This is a challenging task since the nature of plasticity at the nanoscale is not fully understood and is still in need of significant development.

Finally, this study helps elucidate methods to reduce tip wear in AM-AFM. As mentioned above and discussed in detail in the Methods section, parameters were deliberately chosen that were rather harsh in order to produce observable tip wear. In particular, measurements were obtained in the high amplitude/repulsive AM-AFM regime instead of the low amplitude/attractive regime.[48] Furthermore, working in the

low amplitude/attractive regime will lead to lower peak repulsive forces and thus less sample wear, as has been demonstrated previously.[49]

CONCLUSION

We have developed and applied a new AM-AFM wear protocol to study the tip wear of DLC and silicon-nitride-coated probes tapping against a UNCD sample. The protocol enables accurate determination of the interaction forces and elastic stresses considering the complex tip geometry. We have shown how the peak repulsive force and the average elastic normal stress evolve as the tip geometry changes. Our results demonstrate that tip wear can be significant in AM-AFM imaging. The observed evolution of the silicon nitride tips is consistent with plastic deformation and removal of nanoscale fragments; further studies are required to fully validate this. For DLC, a smoother evolved tip profile indicating a more gradual wear process is observed. The results are consistent with atom-by-atom removal, as observed previously.[17,50]

To reduce wear, the AM-AFM user can exercise several choices. First, choosing parameters that reduce the peak repulsive force will reduce wear. Second, choosing a larger tip will reduce stresses. This has the obvious drawback of reducing spatial resolution. However, in some cases, lower spatial resolution may be a worthwhile trade-off if stable, constant observations with AM-AFM are desired. For example, if one seeks to compare the properties of a series of samples using AM-AFM, the comparison will be polluted by a changing tip; working with a larger tip radius will alleviate this problem. Finally, using hard tip materials is beneficial, as seen before for contact mode tips.[13,17,51] We find, under harsh AM-AFM operation conditions, that the overall wear rate of silicon-nitride-coated tips is superior to that of the DLC-coated tips studied here. Advanced materials tolerant to a wide range of environments such as UNCD[13,52] may have potential for such improved performance. Combined with proper selection of AM-AFM operating parameters, AM-AFM operation with significantly extended endurance of the tip is readily attainable.

METHODS

HR-TEM and Blind Tip Reconstruction. As the change in tip geometry is the primary result of tip wear, tracking the evolution of the tip geometry during scanning is crucial. As mentioned previously, the shapes of the AFM tips are generally not simple paraboloids or spheres; therefore, accurate determination of the effective tip radius to be used for force and stress calculations is not straightforward.

There are several ways to measure the tip geometry, including HR-TEM, scanning electron microscopy (SEM), and reverse imaging or BTR. Unfortunately, HR-TEM and SEM are somewhat time-consuming, and depending on conditions and the tip material, prolonged exposure to the electron beam can contaminate the probe being imaged.[53] Here, HR-TEM is used as it captures high-resolution images of the tip apex that is better than what is attainable by SEM, and the HR-TEM profiles can be used to estimate the worn volume and the radius of the tip. Furthermore, care is taken to avoid long exposure times to the electron beam, such that no TEM-induced contamination is observed.

One limitation of this method is that it only provides a two-dimensional profile of the tip since the tip is viewed in the plane transverse to the electron beam. Furthermore, the TEM can only access the plane that is parallel to the axes of the cantilever and the tip (the *y*-direction in Figure 8). A profile along the *x*-direction cannot be obtained since the TEM's electron beam is blocked by the cantilever carrier chip.

A more convenient and rapid technique to determine tip shapes is to perform BTR using a sample with small, random, and durable sharp features, such as the Nioprobe or TipCheck (Aurora NanoDevices Inc.) commercial samples or UNCD, which has fine random features on its surface. The BTR method relies on the fact that an AFM topography image is a convolution of the tip geometry and the surface features. As a result of the finite size of an AFM tip, topographic images do not directly reflect the actual sizes of the sample features, and thus an AFM topographic image contains information regarding the shape of the tip. Image processing, performed here with the commercial software package Scanning Probe Image Processor (SPIP, Image Metrology A/S), can generate a reconstructed image of the tip that was used to obtain the topography image. From this reconstruction, the shape and approximate radius of the tip can be determined in two directions, which correspond to the *x*- and *y*-directions of the topography image. The *x*-direction tip profile determined by BTR gives information about the tip that is not accessible by HR-TEM. Strictly speaking, the tip shape provided corresponds to the largest possible tip that could have generated the recorded image data and thus represents an upper bound on the tip shape. However, good quantitative agreement between BTR and HR-TEM images has been demonstrated.[13,14] The primary disadvantage of BTR is that it only provides information of the tip geometry over a region that is a few nanometers from the tip's apex. Therefore, to determine the tip–sample interacting geometry, we use both HR-TEM imaging and BTR as described below.

As BTR provides information about the portion of the tip that interacts directly with the sample, its *y*-direction profile can be aligned with the HR-TEM image profile to identify the tip apex. However, the HR-TEM image should be rotated as the cantilever carrier chip is mounted in the AFM instrument at an angle, usually 11°, with respect to the sample. This way, one can determine what specific portion of the tip apex is interacting

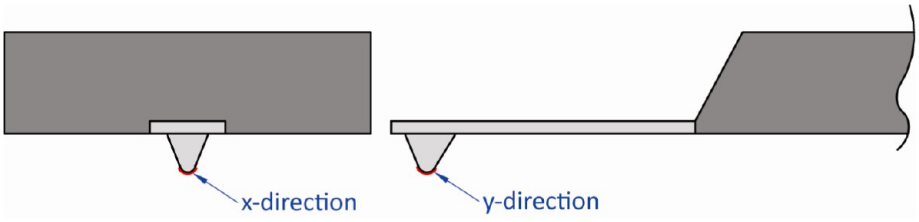

Figure 8. AFM probe tip *x*- and *y*-direction profiles. HR-TEM imaging is only able to capture the *y*-direction profile.

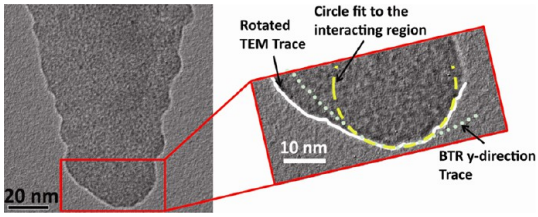

Figure 9. Determination of the effective tip radius (along the *y*-direction profile, $R = R_y$) by combining HR-TEM and BTR.

with the sample during imaging (Figure 9). A circle or parabola can then be fit to the appropriate portion of the tip to determine the effective tip radius of that region. In this work, several reasonable circles and parabolas are fit, and an average radius of these fits is used. This fitting provides the radius of the tip in the direction parallel to the long axis of the cantilever, denoted here as R_y. BTR can be also used to estimate the tip radius in the direction perpendicular to the long axis of the cantilever, denoted here as R_x. However, the accuracy of the tip radius determined by BTR depends on the amount of noise in the height image. Therefore, to estimate R_x, we obtain an image where the fast scan direction is chosen to be perpendicular to the long axis of the cantilever since the tip radius acquired along the fast scan direction is more reliable as it is acquired more quickly and is thus less noisy and subject to less drift than the slow scan direction.

Wear Experiment Protocol. To perform consistent and comparable wear tests on different tip materials, all experiments need to follow a common protocol. For this study, the experimental protocol was developed by adapting a previous contact mode wear test protocol[14] to AM-AFM wear testing. The protocol involves performing pull-off force measurements using a comparable AFM probe to estimate the work of adhesion for the probe tip of interest, controlling the tip−sample attractive/repulsive force regime, calculating maximum contact forces and normal stresses, and quantifying the wear volume using HR-TEM imaging. Figure 10 summarizes the overall AM-AFM wear protocol.

As mentioned above, the work of adhesion is required to calculate peak repulsive force. If the work of adhesion between the tip and sample materials is unknown, pull-off force measurements can be performed using contact mode probes made out of the same materials as the AM-AFM probes. Preferably, contact mode probes from the same vendor, made of the same tip material, where the tip is formed using the same standard process, should be used to ensure that the tip morphology and chemical properties are as similar as possible for both the contact mode and AM-AFM probes. Here, for each tip−sample material pair tested for wear in AM-AFM, three separate contact mode probes, all with identical specifications, from the same vendor as the AM-AFM probes and composed of the same tip material, were used to measure the work of adhesion. A total of 150 force−distance curves (5 different locations on the sample, with 30 force−distance curves taken at each location) were acquired from each probe at 15% relative humidity. The reported work of adhesion, calculated using the DMT contact model, is the average of 450 data points (3 probes with 150 force−distance curves each). As it appears in eq 2, to calculate work of adhesion, one needs to measure the tip radius. Here, HR-TEM images of the contact mode probe tips are obtained to measure the tip geometry and to estimate the effective tip radius both before and after obtaining the force−distance curves. Tips whose geometries deviate substantially from paraboloidal shape are discarded and additional measurements with a new probe acquired. For suitable tips, an average of the tip radius before and after measurements is used. Here, the average change in the tip radius before and after measurements was about 9 nm. This method assumes no significant change in the tip's surface chemistry during AM-AFM wear tests. In fact, tip chemistry could change if contamination or the native oxide layer is removed or modified. Countering this, since the experiments are performed in air, there likely is rapid recontamination from ambient species and reoxidation.

The next step in the protocol involves obtaining HR-TEM images of new, unused AM-AFM probes to determine the initial tip shape and morphology. Once again, tips with unusual shapes or observable contamination are discarded. Then, using the AFM, each cantilever's quality factor and resonance frequency are measured, and its normal force spring constant is determined using the Sader method.[54] The quality factor and resonance frequency are measured by both regular mechanical tuning and by thermal noise spectra using built-in features of the AFM systems. Values obtained from these two methods are theoretically the same[54] and are averaged to provide more reliable measurements. The inverse optical lever sensitivity (InvOLS) of the cantilever's normal deflection signal, which is the conversion factor between the amplitude expressed in volts to nanometers, is required in order to calibrate the amplitude. This is calculated by measuring the thermal noise spectrum of the first flexural mode and fitting it with a Lorentzian function scaled so that it integrates to the thermal energy $k_BT/2$. This scaling is based on the equipartition theorem, which relates the cantilever's Brownian motion of the first flexural mode to its thermal energy.[55] As the spring constant is known through Sader method, the Lorentzian curve fit determines the InvOLS. After characterizing the tips and the cantilevers, the probes were used to scan a UNCD sample ($1 \times 1\ \mu m^2$, 512×512 pixels, 1 Hz scan rate) to obtain a high-quality topography image that can be used for BTR; we call this the BTR scan. UNCD is chosen as the sample because it exhibits sharp, random features that can be used for BTR and is highly wear-resistant, leading to the tip wearing more than the sample. For the BTR scan, the imaging parameters are chosen to avoid any significant tip wear: the free oscillation amplitude is kept small (on the order of a few nanometers), and the amplitude ratio is set as close to 1 as possible while still tracking the topography of the sample. The tip profile extracted from the initial HR-TEM image is compared to that obtained from the BTR scan to determine an initial effective tip radius as described above. The same procedure for determining the tip radius is applied over the course of the entire wear test, using topographic images acquired immediately before TEM imaging for blind tip reconstruction.

To establish and maintain the force regime in which the tip operates during scanning and to determine the peak repulsive force, the free oscillation amplitude and the amplitude ratio are selected and held constant throughout the duration of the wear test. In the present work, wear scans are performed in the high amplitude/repulsive regime. In the following section, the method for determining appropriate amplitude ratios for a given free oscillation amplitude to ensure imaging stability is explained. Once the initial measurements have been obtained and the wear test parameters have been chosen, the wear testing begins. For our studies, we acquired a total of forty-five $1 \times 1\ \mu m^2$ images of a UNCD sample. HR-TEM images of the tips were acquired after 1, 3, 9, 21, and 45 scans. The HR-TEM images, along with BTR analysis of the topographic images, provide information about the evolution of the tip shape and radius throughout the wear test and are used to calculate peak repulsive forces and average normal stresses.

Controlling and Maintaining the Force Regime. The force regime (low amplitude/attractive *vs* high amplitude/repulsive) plays an important role in the wear of AM-AFM probes as the tip−sample interaction forces and dissipated energy will vary depending on the force regime.[48,56] The parameters used for maintaining and controlling the force regime could differ depending on the particular tip and sample materials, cantilever properties, tip morphology, and experimental setup. Usually higher amplitude ratios (*i.e.*, tapping amplitude close to free amplitude) result in attractive regime operation, while low amplitude ratios will lead to repulsive regime operation. For given tip and sample materials, cantilever properties, and free amplitude, there will be a range of amplitude ratios within which transitions between the two force regimes can occur. The range can be found by obtaining amplitude and phase *versus* *z*-position plots using a sacrificial probe of the same type (and nominally of the same tip size and surface chemistry) as that which will be used in the

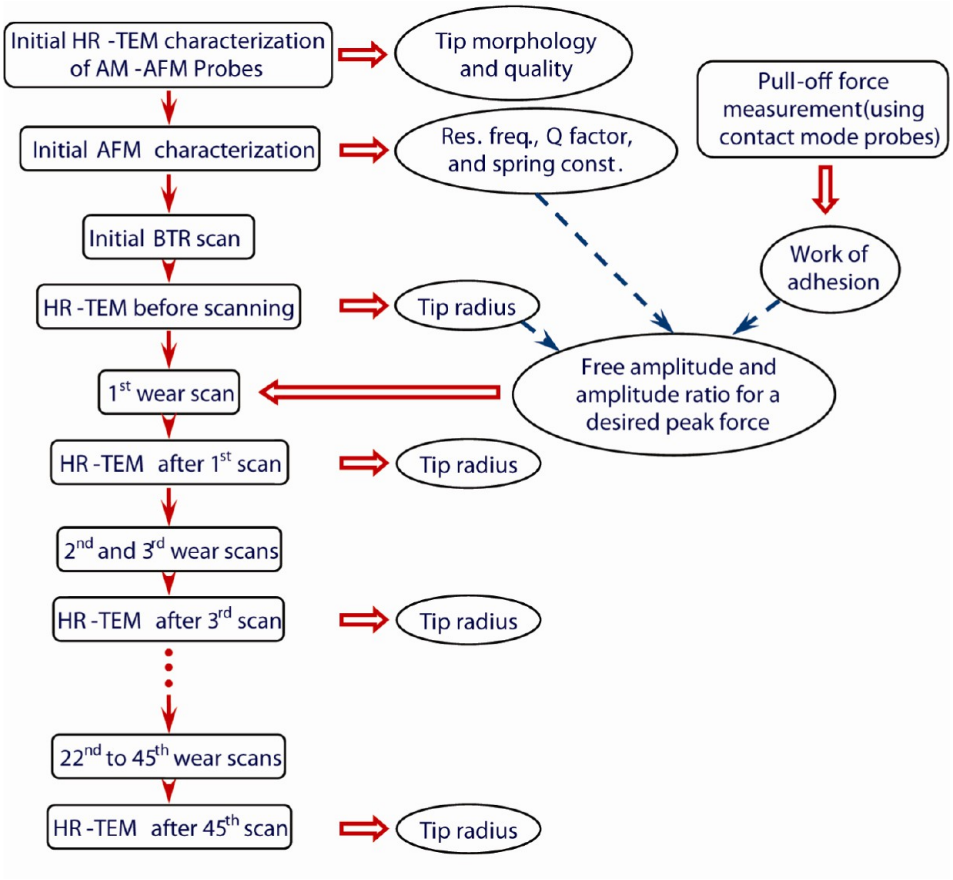

Figure 10. Flowchart illustrating the wear experiment protocol.

experiment. Upon approaching the surface, a transition from the attractive to repulsive regime will be observed; the reverse transition will occur upon retracting from the surface. Working significantly below or above this transition range ensures imaging stability by avoiding the bistable regime.[49] The most straightforward way to determine the force regime while scanning the sample is by examining the phase shift. The phase shift between the excitation signal and the cantilever response in AM-AFM is routinely obtained simultaneously with the topography. Typically, an average phase angle between 0 and −90° (−90 and −180°) is an indication that the system is operating in the repulsive (attractive) regime. Care should be taken as the raw phase angle may not be reported in certain commercial AFM instruments; some systems offset the phase by 90° or change the sign, for example.

Wear Volume Calculation. As an example of the wear volume calculation, Figure 11a shows overlaid profiles of the diamond-like carbon-coated silicon tip. The profiles are obtained from HR-TEM images acquired before scanning and after 1, 3, 9, 21, and 45 scans. A custom MATLAB script is used to trace the edges of the tip boundaries. The 2D profiles are used to approximate the volume of material that has been worn and/or plastically displaced by integrating over the tip profile up to a certain height of the tip shank using the method of disks.[14] This integration approach assumes that the tips are circularly symmetric at each height increment. However, the application of this procedure to the SiN_x-coated tips that exhibit plastic deformation and bulging (flow of the tip materials to the sides, Figure 2) requires careful selection of the integration height. As demonstrated in Figure 11c, the integration height should be just above the worn or plastically deformed region. Also, before determining the integration height, it may be necessary to rotate the overlaid profiles to take advantage of any symmetry of the worn region, as shown in Figure 11b. This rotation is different from the rotation described in the following section which helps to determine the initial point of contact of the actual tip profile and it is solely to avoid integration of the displaced material around the tip apex. This is because the plastic deformation is not necessarily produced evenly on the periphery of the tip. Therefore, if one includes the displaced material in the integration using method of disks, which assumes axisymmetry at any given height, a large error can be introduced to the wear volume calculation.

As demonstrated in Figure 7, to discuss the number of atoms removed due to wear, it is necessary to estimate the number of atoms per cubic nanometer of the wear volume since our tip materials have differing compositions. Using the density and the atomic percentage of hydrogen, one can readily calculate the number of carbon and hydrogen atoms per cubic nanometer of DLC. The DLC coating is estimated to have 41 ± 2 atom % hydrogen content and a density of 1.79 ± 0.1 g/cm^3, based on X-ray reflectivity and secondary ion mass spectroscopy experiments (Evans Analytical Group, Sunnyvale, CA) performed on DLC films deposited on flat substrates using the same deposition system and conditions as the films deposited on the tips. Using these measured values, we estimated there to be 85 ± 1 carbon atoms/nm^3 and 59 ± 5 hydrogen atoms/nm^3 in our DLC. We also included the number of silicon atoms from the original uncoated tip that are removed starting from 9 scans and after in our calculation of the total number of worn atoms. Using 2.33 g/cm^3 as the density of silicon,[57] one can estimate the number of silicon atoms to be 50 ± 1/nm^3. Similarly, there are 40 ± 3 silicon atoms and 53 ± 4 nitrogen atoms/nm^3 assuming 3.1 ± 0.2 g/cm^3 as the silicon nitride density.[58]

Estimation of the Work of Adhesion. Using the procedure described in ref 59 as a first estimate of the work of adhesion, an upper bound to the work of adhesion is obtained by assuming that the JKR model applies; if Maugis' parameter is found to still be in the DMT regime despite this extreme value of the work of adhesion, then the contact is safely in the DMT regime and corrected values for the work of adhesion can be determined.

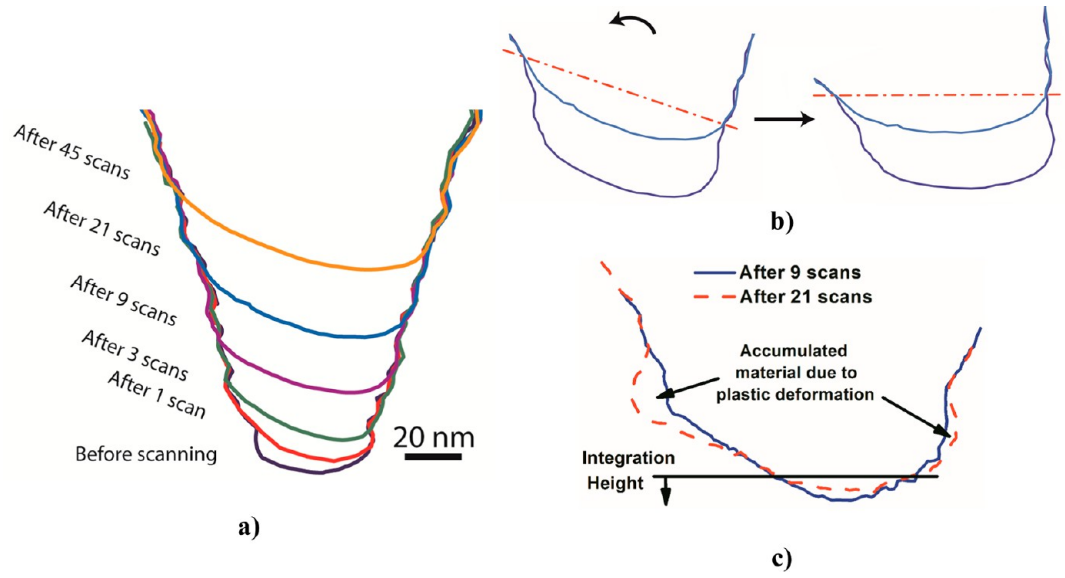

Figure 11. (a) Overlaid HR-TEM profiles of a DLC-coated tip before AM-AFM scanning and after completing 1, 3, 9, 21, and 45 scans. (b) Overlaid HR-TEM profiles of the same DLC-coated tip after 9 and 21 scans, before and after being rotated by 16° so that they are oriented with respect to the horizontal as they are in the AFM. The 16° rotation is particular to these two profiles. The angle for other profiles could be different. The rotated profiles are used for the stress calculations. (c) Overlaid HR-TEM profiles of a SiN_x-coated tip after 9 and 21 scans, showing the height chosen for estimating removed material.

The JKR work of adhesion determined from pull-off force measurements is found to be 42 ± 16 mJ/m^2 between the DLC tip and the UNCD sample and 48 ± 25 mJ/m^2 between the silicon nitride tip and UNCD. The reported error is based on the standard deviation of all the pull-off force measurements taken initially for a given tip and propagating the error determined from the tip radius measurement. We believe that the substantial standard deviation comes from the fact that the UNCD surface is rough and inhomogeneous. The inhomogeneity could be structural in origin as UNCD is made out of randomly oriented grains composed of sp^3-bonded C atoms and grain boundaries composed of a mixture of sp^2- and sp^3-bonded C atoms. It may also have a chemical origin, as the local chemical termination of the UNCD may involve hydrogen atoms, hydroxyl groups, or other species as affected by modest amounts of contamination that are inevitable upon exposing a sample to ambient conditions. Therefore, depending on where the AFM tip lands, the pull-off forces will vary. In addition, the variation may also arise from UNCD surface roughness, in which case the assumption of a paraboloidal tip interacting with a flat surface used for all of the contact mechanics analysis in this study will introduce error. To address this, we performed roughness analysis on the tip and sample surfaces within the scale of the tip−sample contact area. To assess the roughness of the UNCD sample, we analyzed high-resolution topographic AFM images that were 200 × 200 nm^2 in area with 2048 scanning lines and 2048 pixels per line (*i.e.*, every pixel is less than 1 × 1 Å^2 in size). We then corrected the image by reducing the effect of tip convolution using the tip deconvolution algorithm of the SPIP software. From this, we analyzed a series of 5 nm long line profiles to extract the rms roughness of the sample. For each tip, as described before, we fit a parabola to the tip profile captured from TEM imaging and then subtracted that parabola from the actual tip profile over a 5 nm range centered at the tip's apex (*i.e.*, the region over which tip−sample contact is made). The roughness of the profile that resulted from the subtraction was then calculated to obtain a roughness value that would be equivalent to that of a flat surface. We chose the value of 5 nm based on the calculated contact diameters, which ranged from 1.3 to 4.3 nm according to our contact mechanics modeling; thus, 5 nm is a conservative upper bound to the possible contact diameter. The calculated rms roughness of the UNCD profiles ranged from below 0.3 nm (within the noise limit of the AFM) to a maximum of 0.9 nm, while the calculated rms roughness of the tips ranged from 0.2 to 0.5 nm. The true work of adhesion is going to be larger than what we extract from calculations assuming a parabolic tip and a flat sample. Thus, our values (calculated in the following paragraph) are lower bounds. However, this does not necessarily mean that the real adhesion force that the AFM tips feel is larger than what we estimated here from pull-off force measurements. The pull-off force measurements necessarily involve the tip and sample roughness, and whatever we measure in the force−distance curves will be a good representation of what AFM probes experience in the subsequent AM-AFM mode measurement. The problem with tip and sample roughness is that we use the DMT model, which assumes no roughness, to relate a pull-off force obtained with a slightly rough tip and sample to an effective work of adhesion (not true work of adhesion); we then use that effective work of adhesion to estimate the pull-off force that other rough tips with different global radii experience. If the roughness varies substantially between different tips, then this will introduce error.[60] The ideal approach would be to replace the DMT model with a model that takes into account the contacting bodies' roughness. Unfortunately, no reliable method for that exists, and even if it did, it would require frequent measurement of the evolving tip roughness and the local sample roughness. At this time, such an undertaking is beyond the state-of-the-art for any practical AFM applications (the only report dealing with this issue required combining *in situ* TEM measurements of contact with detailed atomistic simulations[60]). Given that the roughness of all of the tips varies within a reasonable narrow range, from 0.2 to 0.5 nm, the error introduced will not dramatically alter our conclusions.

As discussed before, to determine which contact mechanics model is most appropriate, the Maugis' parameter, λ, and the nondimensional load, $\bar{P}$, are calculated as follows:[34]

$$\lambda = 1.16\left(\frac{Rw^2}{E^{*2}z_0^3}\right)^{1/3} \quad (4)$$

$$\bar{P} = \frac{P}{\pi w R} \quad (5)$$

where z_0 is the equilibrium separation and P is the normal load, which in this case is the peak repulsive force. For the DLC-coated probe, the average peak repulsive force is 90 nN, the average tip radius is 50 nm, and we choose z_0 = 0.3 nm, a reasonable value

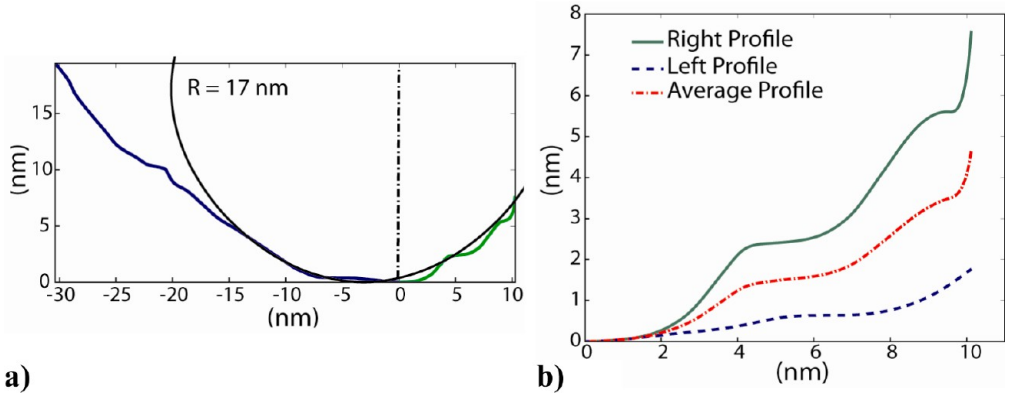

Figure 12. (a) Profile of an AFM tip apex with a fitted circle, $R = 17$ nm. (b) Right profile, left profile (mirrored), and the average profile of the tip apex, used for constructing the three different axisymmetric tip shapes.

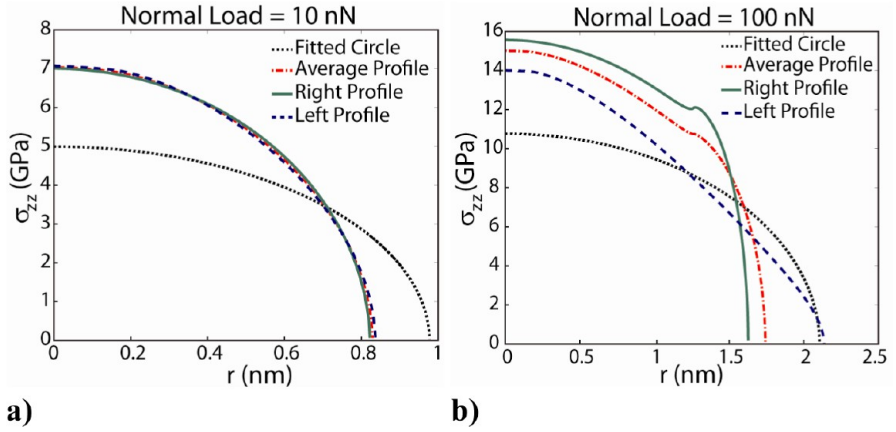

Figure 13. Normal stress distributions at the contact of the left, right, and average profiles of the tip apex and the fitted circle in Figure 12 for (a) 10 and (b) 100 nN normal loads.

used for the equilibrium separation. Using eqs 4 and 5, λ is approximately 0.06 and $\bar{P}$ is found to be 14. For the silicon-nitride-coated probes, the average peak repulsive force is 46 nN and the average tip radius is 27 nm. Likewise, λ is calculated to be approximately 0.05, and $\bar{P}$ is approximately 11. According to the adhesion map (Figure 5 of ref 34), the contact mechanics of both cases of DLC-coated and silicon-nitride-coated probes against UNCD are best described by the DMT model. This holds despite using upper-level estimates for the work of adhesion (*i.e.*, the JKR equation provides lower-level values for $\bar{P}$ and higher-level values for λ, but the transition from the DMT to JKR limit strongly depends on the value of λ). Therefore, the work of adhesion values can be corrected using the DMT equation. From this, one finds the DMT work of adhesion based on measurements with contact mode tips for DLC-UNCD to be 31 ± 12 mJ/m^2 and silicon nitride-UNCD to be 36 ± 19 mJ/m^2. The values are then used for calculating the peak repulsive force and contact stress in subsequent wear experiments.

Average Normal Stress of an Arbitrarily Shaped AFM Tip. As the AFM tip apexes are not simple smooth paraboloids, it is important to consider the difference between the stress calculated by simply fitting a paraboloid to the tip apex and the stress calculated using a line fit to the actual tip profile. As mentioned earlier, we use the solution presented by Zhou *et al.*[35] for an axisymmetric arbitrary punch shape. It is important to determine the point in the profile estimated to be the point of initial contact with the sample and the profile's correct orientation with respect to the sample. This is performed by examining the overlaid HR-TEM images (Figure 11a). It is apparent that the tip is not worn evenly about its axis of symmetry as there is more wear toward the left side of the tip shank. This is more obvious in the case of the tip profiles of the two successive HR-TEM images in Figure 11b. As mentioned before, this is primarily a result of the probe chip being mounted in the AFM instrument at an angle, in this case 11°, with respect to the sample. This mounting angle does not necessarily determine the true tip–sample orientation as the presence of any contamination between the chip and the chip holder, any slope in the cantilever with respect to the chip, or any slope in the sample's surface with respect to the AFM stage can alter the angle somewhat. Therefore, rotating the tip profiles until the worn region is symmetric (Figure 11b) provides a better approximation of the tip profile orientation with respect to the sample. In the case shown in Figure 11b, the orientation angle is determined to be 16°, which is particular to these two profiles. The angle for other profiles could be different, and in this study ranged from 8 to 22° including the total variation seen among all three tips. For any given tip, this range was smaller. For example, for the DLC tip, this range was 15 to 17°. Consequently, the lowest point in the rotated initial tip profile is then assumed to be the point of initial contact. Here, one might argue that the slight relative motion (and consequent shear stress) between the tip and sample along the cantilever long axis can significantly contribute to the asymmetry of the worn region. A simple geometrical consideration of the worst-case scenario here, which is the case of the DLC-coated tip with largest tip–sample deformation (≈0.5 nm), reveals that the largest tip–sample relative motion is about 1 Å, less than the length of an atomic bond. Therefore, the resulting shear strain is insignificant.

Another challenge in applying the method of Zhou *et al.* is that, even after performing this rotation, the tip apex's profile will most likely not have mirror symmetry about the vertical axis. Figure 12a shows how the left side of a DLC-coated silicon tip apex is different from its right side. To address this, one can

consider three different axisymmetric tip profiles (Figure 12b); one is constructed with the left side of the profile, the other one with the right side, and the third tip is the average of the left and right profiles. Here, we use the average profile to then calculate the average normal interfacial contact stress, which is calculated by dividing the total applied normal load, which is the peak repulsive force plus adhesion force, by the contact area. The stress values extracted from left and right profiles are used to calculate the range of uncertainty.

The normal stress distribution at the contact of these three profiles and a circle fit to the tip apex (Figure 12a) are plotted in Figure 13 for 10 and 100 nN applied normal loads. It is apparent that the stress distribution of the fitted circle is quite different from that of the profiles determined from the actual geometry. For the case of the 10 nN applied load, the stress distribution of the left, right, and average profiles are similar due to the fact that the tip profiles are quite similar within the contact radius, which is less than 1 nm. However, these stress distributions begin to deviate from one another in the case of the 100 nN applied load because the tip profiles begin to be different as we move further in the radial direction. This justifies our selection of the average of the actual tip profile (with the left and right portions of the profile used for the uncertainty limits) in addition to fitting a circle or parabola for estimating the average normal contact stress.

Conflict of Interest: The authors declare no competing financial interest.

Acknowledgment. This work was supported by NSF under awards CMMI-0826076, CMMI-0825000, and GOALI/CMMI-1200019, and STTR Grants IIP-0638030 and IIP-0823002, and was partially supported by the Nano/Bio Interface Center through the national science foundation NSEC DMR08-32802. Use of University of Pennsylvania Nano/Bio Interface Center instrumentation is acknowledged. We thank A. Raman, T.D.B. Jacobs, and Graham E. Wabiszewski for useful and stimulating discussions. We thank K. Sridharan for providing the DLC-coated probes.

REFERENCES AND NOTES

1. Binnig, G.; Quate, C. F.; Gerber, C. Atomic Force Microscope. *Phys. Rev. Lett.* **1986**, *56*, 930–933.
2. Liu, Z.; Li, Z.; Wei, G.; Song, Y.; Wang, L.; Sun, L. Manipulation, Dissection, and Lithography Using Modified Tapping Mode Atomic Force Microscope. *Microsc. Res. Tech.* **2006**, *69*, 998–1004.
3. Wang, Y.; Hong, X.; Zeng, J.; Liu, B.; Guo, B.; Yan, H. AFM Tip Hammering Nanolithography. *Small* **2009**, *5*, 477–483.
4. Paolicelli, G.; Mougin, K.; Vanossi, A.; Valeri, S. Adhesion Detachment and Movement of Gold Nanoclusters Induced by Dynamic Atomic Force Microscopy. *J. Phys.: Condens. Matter* **2008**, *20*, 354011.
5. Martínez, N. F.; Kamiński, W.; Gómez, C. J.; Albonetti, C.; Biscarini, F.; Pérez, R.; García, R. Molecular Scale Energy Dissipation in Oligothiophene Monolayers Measured by Dynamic Force Microscopy. *Nanotechnology* **2009**, *20*, 434021.
6. Dietz, C.; Zerson, M.; Riesch, C.; Franke, M.; Magerle, R. Surface Properties of Elastomeric Polypropylenes Studied with Atomic Force Microscopy. *Macromolecules* **2008**, *41*, 9259–9266.
7. Solares, D. Characterization of Deep Nanoscale Surface Trenches with AFM Using Thin Carbon Nanotube Probes in Amplitude-Modulation and Frequency-Force-Modulation Modes. *Meas. Sci. Technol* **2008**, *19*, 015503.
8. Martin, Y.; Williams, C. C.; Wickramasinghe, H. K. Atomic Force Microscope-Force Mapping and Profiling on a Sub 100-Å Scale. *J. Appl. Phys.* **1987**, *61*, 4723.
9. Johnson, K. L. Normal Contact of Elastic Solids: Hertz Theory. In *Contact Mechanics*; Cambridge University Press: Cambridge, UK, 1985; pp 84−106.
10. Johnson, K. L.; Kendall, K.; Roberts, A. D. Surface Energy and the Contact of Elastic Solid. *Proc. R. Soc. London, Ser. A* **1971**, *324*, 301–313.
11. Derjaguin, B. V.; Muller, V. M.; Toporov, Yu. P. Effect of Contact Deformations on the Adhesion of Particles. *J. Colloid Interface Sci.* **1975**, *53*, 314–326.
12. Luan, B.; Robbins, M. The Breakdown of Continuum Models for Mechanical Contacts. *Nature* **2005**, *435*, 929–932.
13. Liu, J.; Grierson, D. S.; Notbohm, J.; Li, S.; O'Connor, S. D.; Turner, K. T.; Carpick, R. W.; Jaroenapibal, P.; Sumant, A. V.; Carlisle, J. A.; *et al.* Preventing Nanoscale Wear of Atomic Force Microscopy through the use of Monolithic Ultrananocrystalline Diamond Probes. *Small* **2010**, *6*, 1140–1149.
14. Liu, J.; Notbohm, J. K.; Carpick, R. W.; Turner, K. T. Method for Characterizing Nanoscale Wear of Atomic Force Microscope Tips. *ACS Nano* **2010**, *4*, 3763–3772.
15. Fletcher, P. C.; Felts, J. R.; Dai, Z.; Jacobs, T. D.; Zeng, H.; Lee, W.; Sheehan, P. E.; Carlisle, J. A.; Carpick, R. W.; King, W. P. Wear-Resistant Diamond Nanoprobe Tips with Integrated Silicon Heater for Tip-Based Nanomanufacturing. *ACS Nano* **2010**, *4*, 3338–3344.
16. Gotsmann, B.; Lantz, M. A. Atomistic Wear in a Single Asperity Sliding Contact. *Phys. Rev. Lett.* **2008**, *101*, 125501-4.
17. Bhaskaran, H.; Gotsmann, B.; Sebastian, A.; Drechsler, U.; Lantz, M.; Despont, M.; Jaroenapibal, P.; Carpick, R. W.; Chen, Y.; Sridharan, K. Ultra-low Nanoscale Wear through Atom-by-Atom Attrition in Silicon-Containing Diamond-like Carbon. *Nat. Nanotechnol.* **2010**, *5*, 181–185.
18. Jacobs, T. D.; Gotsmann, B.; Lantz, M. A.; Carpick, R. W. On the Application of Transition State Theory to Atomic-Scale Wear. *Tribol. Lett.* **2010**, *39*, 257.
19. Ho, H. J. Near-Contact Mode: A Novel AFM Operation Mode for Non-destructive, Ultra-high Lateral Resolution Topography Measurement in Air. *Proc. SPIE* **1998**, *3512*, 40–53.
20. Chung, K.-H.; Lee, Y.-H.; Kim, D.-E.; Yoo, J.; Hong, S. Tribological Characteristics of Probe Tip and PZT Media for AFM-Based Recording Technology. *IEEE Trans. Magn.* **2005**, *41*, 849–854.
21. Nie, H.-Y.; McIntyre, N. S. Unstable Amplitude and Noisy Image Induced by Tip Contamination in Dynamic Force Mode Atomic Force Microscopy. *Rev. Sci. Instrum.* **2007**, *78*, 023701.
22. Kim, H. J.; Moldovan, N.; Felts, J. R.; Somnath, S.; Dai, Z.; Jacobs, T. D.; Carpick, R. W.; Carlisle, J. A.; King, W. P. Ultrananocrystalline Diamond Tip Integrated onto a Heated Atomic Force Microscope Cantilever. *Nanotechnology* **2012**, *23*, 495302/1-9.
23. Fletcher, P. C.; Felts, J. R.; Dai, Z.; Jacobs, T. D.; Zeng, H.; Lee, W.; Sheehan, P. E.; Carlisle, J. A.; Carpick, R. W.; King, W. P. Wear-Resistant Diamond Nanoprobe Tips with Integrated Silicon Heater for Tip-Based Nanomanufacturing. *ACS Nano* **2010**, *4*, 3338–3344.
24. Qian, L. M.; Xiao, X. D.; Wen, S. Z. Tip *In Situ* Chemical Modification and Its Effects on Tribological Measurements. *Langmuir* **2000**, *16*, 662–670.
25. Doris, B. B.; Hegde, R. I. Improved Atomic Force Microscopy Imaging Using Carbon-Coated Probe Tips. *Appl. Phys. Lett.* **1995**, *67*, 3816–3818.
26. Larsen, T.; Moloni, K.; Flack, F.; Eriksson, M. A.; Lagally, M. G.; Black, C. T. Comparison of Wear Characteristics of Etched-Silicon and Carbon Nanotube Atomic-Force Microscopy Probes. *Appl. Phys. Lett.* **2002**, *80*, 1996–1998.
27. Su, C.; Huang, L.; Kjoller, K.; Babcock, K. Studies of Tip Wear Processes in AM-AFM Atomic Force Microscopy. *Ultramicroscopy* **2003**, *97*, 135–144.
28. Bassani, R.; D'Acunto, M. Nanotribology: Tip-Sample Wear under Adhesive Contact. *Tribol. Int.* **2000**, *33*, 443–452.
29. Katan, A. J.; van Es, M. H.; Oosterkamp, T. H. Quantitative Force *versus* Distance Measurements in Amplitude Modulation AFM: A Novel Force Inversion Technique. *Nanotechnology* **2009**, *20*, 165703.
30. Sader, J. E.; Uchihashi, T.; Higgins, M. J.; Farrell, A.; Nakayama, Y.; Jarvis, S. P. Quantitative Force Measurements Using Frequency Modulation Atomic Force Microscopy-Theoretical Foundations. *Nanotechnology* **2005**, *16*, S94–101.
31. Katan, A. J. Exploring the Limits of Amplitude Modulation Force Spectroscopy with Numerical Experiments. In Measuring Interactions in Fluids with Small-Cantilever AFM; PhD Thesis, Leiden University, Leiden, Netherlands, 2007; pp 65−82.

32. Hu, S. Analytical Formulas and Scaling Laws for Peak Interaction Forces in Dynamic Atomic Force Microscopy. In Nonlinear Dynamics and Force Spectroscopy in Dynamic Atomic Force Microscopy; PhD Thesis, Purdue University, West Lafayette, IN, 2007; pp 74−101.
33. Melcher, J.; Kiracofe, D.; Hu, S.; Raman, A. VEDA 2.0 (Virtual Environment for Dynamic AFM) http://nanohub.org/resources/adac 2012.
34. Johnson, K. L.; Greenwood, J. A. An Adhesion Map for the Contact of Elastic Spheres. *J. Colloid Interface Sci.* **1997**, *192*, 326–333.
35. Zhou, S.-S.; Gao, X.-L.; He, Q.-C. A Unified Treatment of Axisymmetric Adhesive Contact Problems Using the Harmonic Potential Function Method. *J. Mech. Phys. Solids* **2011**, *59*, 145–159.
36. Bares, J. A.; Sumant, A. V.; Grierson, D. S.; Carpick, R. W.; Sridharan, K. Small Amplitude Reciprocating Wear Performance of Diamond-like Carbon Films: Dependence of Film Composition and Counterface Material. *Tribol. Lett.* **2007**, *27*, 79–88.
37. Adiga, V. P.; Sumant, A. V.; Suresh, S.; Gudeman, C.; Auciello, O.; Carlisle, J. A.; Carpick, R. W. Mechanical Stiffness and Dissipation in Ultrananocrystalline Diamond Microresonators. *Phys. Rev. B* **2009**, *79*, 245403.
38. Marques, F. C.; Lacerda, R. G.; Champi, A.; Stolojan, V.; Cox, D. C.; Silva, S. R. P. Thermal Expansion Coefficient of Hydrogenated Amorphous Carbon. *Appl. Phys. Lett.* **2003**, *83*, 3099.
39. Khan, A.; Philip, J.; Hess, P. Young's Modulus of Silicon Nitride Used in Scanning Force Microscope Cantilevers. *J. Appl. Phys.* **2004**, *95*, 1667–1672.
40. Dai, C.; Chang, Y. A Resonant Method for Determining Mechanical Properties of Si_3N_4 and SiO_2 Thin Films. *Mater. Lett.* **2007**, *61*, 3089–3092.
41. Chuang, W.-H.; Luger, T.; Fettig, R. K.; Ghodssi, R. Mechanical Property Characterization of LPCVD Silicon Nitride Thin Films at Cryogenic Temperatures. *J. Microelectromech. Syst.* **2004**, *13*, 870–879.
42. Edwards, R. L.; Coles, G.; Sharpe, W. N., Jr. Comparison of Tensile and Bulge Tests for Thin-Film Silicon Nitride. *Exp. Mech.* **2004**, *44*, 49–54.
43. Martyniuk, M.; Musca, C. A.; Dell, J. M. Elasto-Plastic Characterization of Low-Temperature Plasma-Deposited Silicon Nitride Thin Films Using Nanoindentation. *Int. J. Surf. Sci. Eng.* **2009**, *3*, 3–22.
44. Matoy, K.; Schönherr, H.; Detzel, T.; Schöberl, T.; Pippan, R.; Motz, C.; Dehm, G. A Comparative Micro-Cantilever Study of the Mechanical Bahavior of Silicon Based Passivation Films. *Thin Solid Films* **2009**, *518*, 247–256.
45. Martyniuk, M.; Antoszewski, J.; Walmsley, B. A; Musca, C. A.; Dell, J. M.; Jung, Y.-G.; Lawn, B. R.; Huang, H.; Faraone, L. Determination of Mechanical Properties of Silicon Nitride Thin Films Using Nanoindentation. *Proc. SPIE* **2005**, *5798*, 216–225.
46. Merle, B.; Göken, M. Fracture Toughness of Silicon Nitride Thin Films of Different Thicknesses as Measured by Bulge Tests. *Acta Mater.* **2011**, *59*, 1772–1779.
47. Nastasi, M.; Kodali, P.; Walter, K. C.; Embury, J. D.; Raj, R.; Nakamura, Y. Fracture Toughness of Diamond-like Carbon Coatings. *J. Mater. Res.* **1999**, *14*, 2173–2180.
48. García, R.; Paulo, A. S. Attractive and Repulsive Tip−Sample Interaction Regimes in Tapping-Mode Atomic Force Microscopy. *Phys. Rev. B* **1999**, *60*, 4961–4967.
49. García, R.; Pérez, R. Dynamic Atomic Force Microscopy Methods. *Surf. Sci. Rep.* **2002**, *47*, 197–301.
50. Jiang, J.; Arnell, R. The Effect of Sliding Speed on Wear of Diamond-like Carbon Coatings. *Wear* **1998**, *218*, 223–31.
51. Lantz, M. A.; Gotsmann, B.; Jaroenapibal, P.; Jacobs, T. D. B.; O'Connor, S. D.; Sridharan, K.; Carpick, R. W. Wear-Resistant Nanoscale Silicon Carbide Tips for Scanning Probe Applications. *Adv. Funct. Mater.* **2012**, *22*, 1639–1645.
52. Moldovan, N.; Dai, Z.; Zeng, H.; Carlisle, J. A.; Jacobes, T. D. B.; Vahdat, V.; Grierson, D. S.; Liu, J.; Turner, K. T.; Carpick, R. W. Advances in Manufacturing of Molded Tips for Scanning Probe Microscopy. *J. Microelectromech. Syst.* **2012**, *21*, 431–442.
53. Horiuchi, S.; Hanada, T.; Ebisawa, M.; Matsuda, Y.; Kobayashi, M.; Takahara, A. Contamination-Free Transmission Electron Microscopy for High-Resolution Carbon Elemental Mapping of Polymers. *ACS Nano* **2009**, *3*, 1297–1304.
54. Sader, J. E.; Chon, J. W. M.; Mulvaney, P. Calibration of Rectangular Atomic Force Microscope Cantilevers. *Rev. Sci. Instrum.* **1999**, *70*, 3967–3969.
55. Hutter, J. L.; Bechhoefer, J. Calibration of Atomic-Force Microscope Tips. *Rev. Sci. Instrum.* **1993**, *67*, 1868–1873.
56. Martínez, N. F.; García, R. Measuring Phase Shifts and Energy Dissipation with Amplitude Modulation Atomic Force Microscopy. *Nanotechnology* **2006**, *17*, S167–S172.
57. Hammond, C. R. The Elements. In *Handbook of Chemistry and Physics*, 52nd ed.; Weast, R. C., Ed.; CRC: Cleveland, OH, 1971−1972; p B-29.
58. Howard-Knight, J. P.; Hobbs, J. K. Finite Element Modeling of Atomic Force Microscopy Cantilever Dynamics during Video Rate Imaging. *J. Appl. Phys.* **2011**, *109*, 074309.
59. Grierson, D.; Flater, E. E.; Carpick, R. W. Accounting for the JKR-DMT Transition in Adhesion and Friction Measurements with Atomic Force Microscopy. *J. Adhes. Sci. Technol.* **2005**, *19*, 291–311.
60. Jacobs, T. D. B.; Ryan, K. E.; Keating, P. L.; Grierson, D. S.; Lefever, J. A.; Turner, K. T.; Harrison, J. A.; Carpick, R. W. The Effect of Atomic-Scale Roughness on the Adhesion of Nanoscale Asperities: A Combined Simulation and Experimental Investigation. *Tribol. Lett.* **2013**, *50*, 81–93.

Correction to Mechanics of Interaction and Atomic-Scale Wear of Amplitude Modulation Atomic Force Microscopy Probes

[*ACS Nano* **2013,** *7*, 3221–3235. DOI: 10.1021/nn305901n]. Vahid Vahdat, David S. Grierson, Kevin T. Turner, and Robert W. Carpick*

In the Methods section of our article, the statement "*P* is the normal load, which in this case is the peak repulsive force" following equation 5 should be replaced with "*P* is the total normal load, which here should be taken as $F^{rep}_{peak} - F_{adhesion}$".

This erratum does not affect any of the experimental results, discussions, or conclusions reported in the paper. The authors apologize for this unintended oversight.

Published online October 31, 2013
10.1021/nn405606y